Chander, G., Markham, B.L., Helder, D.L. (2009). Summary of Current Radiometric Calibration Coefficients for Landsat MSS, TM, ETM+, and EO-1 ALI Sensors. *Remote Sensing of Environment* 113 (2009) 893–903.

Summary of Current Radiometric Calibration Coefficients for Landsat MSS, TM, ETM+, and EO-1 ALI Sensors

Gyanesh Chander[a], Brian L. Markham[b], Dennis L. Helder[c]

[a] SGT, Inc.[!] contractor to the U.S. Geological Survey (USGS) Earth Resources Observation and Science (EROS) Center, Sioux Falls, SD 57198-0001 USA. [!]Work performed under USGS contract 08HQCN0005 Telephone: 605-594-2554, Email: gchander@usgs.gov

[b] National Aeronautics and Space Administration (NASA) Goddard Space Flight Center (GSFC), Greenbelt, MD 20771, USA

[c] South Dakota State University (SDSU), Brookings, SD 57007, USA

Abstract

This paper provides a summary of the current equations and rescaling factors for converting calibrated Digital Numbers (DNs) to absolute units of at-sensor spectral radiance, Top-Of-Atmosphere (TOA) reflectance, and at-sensor brightness temperature. It tabulates the necessary constants for the Multispectral Scanner (MSS), Thematic Mapper (TM), Enhanced Thematic Mapper Plus (ETM+), and Advanced Land Imager (ALI) sensors. These conversions provide a basis for standardized comparison of data in a single scene or between images acquired on different dates or by different sensors. This paper forms a needed guide for Landsat data users who now have access to the entire Landsat archive at no cost.

Keywords: Landsat, MSS, TM, ETM+, EO-1 ALI, $LMIN_\lambda$, $LMAX_\lambda$, $ESUN_\lambda$, LPGS, NLAPS, Gain, Bias, Calibration, Spectral Radiance, Reflectance, Temperature

1. Introduction

The Landsat series of satellites provides the longest continuous record of satellite-based observations. As such, Landsat is an invaluable resource for monitoring global change and is a primary source of medium spatial resolution Earth observations used in decision-making (Fuller et al., 1994; Townshend et al., 1995; Goward et al., 1997; Vogelmann et al., 2001; Woodcock et al., 2001; Cohen et al., 2004; Goward et al., 2006; Masek et al., 2008; Wulder et al., 2008). To meet observation requirements at a scale revealing both natural and human-induced landscape changes, Landsat provides the only inventory of the global land surface over time on a seasonal basis (Special issues on Landsat, 1984; 1985; 1997; 2001; 2003; 2004; 2006). The Landsat Program began in early 1972 with the launch of the first satellite in the series. As technological capabilities increased, so did the amount and quality of image data captured by the various sensors onboard the satellites. Table 1 presents general information about each Landsat satellite.

Landsat satellites can be classified into three groups, based on sensor and platform characteristics. The first group consists of Landsat 1 (L1), Landsat 2 (L2), and Landsat 3 (L3), with the Multispectral Scanner (MSS) sensor and the Return Beam Vidicon (RBV) camera as payloads on a “NIMBUS-like” platform. The spatial resolution of the MSS sensor was

approximately 79 m (but often processed to pixel size of 60 m), with four bands ranging from the visible blue to the Near-Infrared (NIR) wavelengths. The MSS sensor on L3 included a fifth band in the thermal infrared wavelength, with a spectral range from 10.4 to 12.6 μm. The L1–L3 MSS sensors used a band-naming convention of MSS-4, MSS-5, MSS-6, and MSS-7 for the blue, green, red, and NIR bands, respectively (Markham & Barker, 1983). This designation is obsolete, and to be consistent with the TM and ETM+ sensors, the MSS bands are referred to here as Bands 1–4, respectively.

The second group includes Landsat 4 (L4) and Landsat 5 (L5), which carry the Thematic Mapper (TM) sensor, as well as the MSS, on the Multimission Modular Spacecraft. This second generation of Landsat satellites marked a significant advance in remote sensing through the addition of a more sophisticated sensor, improved acquisition and transmission of data, and more rapid data processing at a highly automated processing facility. The MSS sensor was included to provide continuity with the earlier Landsat missions, but TM data quickly became the primary source of information used from these satellites because the data offered enhanced spatial, spectral, radiometric, and geometric performance over data from the MSS sensor. The TM sensor has a spatial resolution of 30 m for the six reflective bands and 120 m for the thermal band. Because there are no onboard recorders on these sensors, acquisitions are limited to real-time downlink only.

The third group consists of Landsat 6 (L6) and Landsat 7 (L7), which include the Enhanced Thematic Mapper (ETM) and the Enhanced Thematic Mapper Plus (ETM+) sensors, respectively. No MSS sensors were included on either satellite. Landsat 6 failed on launch. The L7 ETM+ sensor has a spatial resolution of 30 m for the six reflective bands, 60 m for the thermal band, and includes a panchromatic (pan) band with a 15 m resolution. L7 has a 378 gigabit (Gb) Solid State Recorder (SSR) that can hold 42 minutes (approximately 100 scenes) of sensor data and 29 hours of housekeeping telemetry concurrently (L7 Science Data User's Handbook[1]).

The Advanced Land Imager (ALI) onboard the Earth Observer-1 (EO-1) satellite is a technology demonstration that serves as a prototype for the Landsat Data Continuity Mission (LDCM). The ALI observes the Earth in 10 spectral bands; nine spectral bands have a spatial resolution of 30 m, and a pan band has a spatial resolution of 10 m.

The Landsat data archive at the U.S. Geological Survey (USGS) Earth Resources Observation and Science (EROS) Center holds an unequaled 36-year record of the Earth's

[1] http://landsathandbook.gsfc.nasa.gov/handbook.html, Landsat Project Science Office, Goddard Space Flight Center.

surface and is available at no cost to users via the Internet (Woodcock et al., 2008). Users can access and search the Landsat data archive via the EarthExplorer (EE)[2] or Global Visualization Viewer (GloVis)[3] web sites. Note that the Landsat scenes collected by locations within the International Ground Station (IGS) network may be available only from the particular station that collected the scene.

2. Purpose

Equations and parameters to convert calibrated Digital Numbers (DNs) to physical units, such as at-sensor radiance or Top-Of-Atmosphere (TOA) reflectance, have been presented in a "sensor-specific" manner elsewhere, e.g., MSS (Markham & Barker, 1986, 1987; Helder, 1993), TM (Chander & Markham, 2003; Chander et al., 2007), ETM+ (Handbook[1]), and ALI (Markham et al., 2004a). This paper, however, tabulates the necessary constants for all of the Landsat sensors in one place defined in a consistent manner and provides a brief overview of the radiometric calibration procedure summarizing the current accuracy of the at-sensor spectral radiances obtained after performing these radiometric conversions on standard data products generated by U.S. ground processing systems.

3. Radiometric calibration procedure

The ability to detect and quantify changes in the Earth's environment depends on sensors that can provide calibrated (known accuracy and precision) and consistent measurements of the Earth's surface features through time. The correct interpretation of scientific information from a global, long-term series of remote-sensing products requires the ability to discriminate between product artifacts and changes in the Earth processes being monitored (Roy et al., 2002). Radiometric characterization and calibration is a prerequisite for creating high-quality science data, and consequently, higher-level downstream products.

3.1. MSS sensors

Each MSS sensor incorporates an Internal Calibrator (IC) system, consisting of a pair of lamp assemblies (for redundancy) and a rotating shutter wheel. The shutter wheel includes a mirror and a neutral density filter that varies in transmittance with rotation angle. The calibration system output appears as a light pulse at the focal plane that rises rapidly and then decays slowly. This pulse is referred to as the calibration wedge (Markham & Barker, 1987). The radiometric calibration of the MSS sensors is performed in two stages. First, raw data from Bands 1–3 are "decompressed" or linearized and rescaled to 7 bits using fixed look-up tables. The look-

[2] http://earthexplorer.usgs.gov

[3] http://glovis.usgs.gov

up tables are derived from prelaunch measurements of the compression amplifiers. Second, the postlaunch gain and offset for each detector of all four bands are individually calculated by a linear regression of the detector responses to the samples of the in-orbit calibration wedge with the prelaunch radiances for these samples. A reasonable estimate of the overall calibration uncertainty of each MSS sensor at-sensor spectral radiances is ±10%, which was the specified accuracy for the sensor (Markham & Barker, 1987). In most cases, the ground processing system must apply an additional step to uncalibrate the MSS data because a number of MSS scenes were archived as radiometrically corrected products. The previously calibrated archived MSS data must be transformed back into raw DNs using the coefficients stored in the data before applying the radiometric calibration procedure. Studies are underway to evaluate the MSS calibration consistency and provide post-calibration adjustments of the MSS sensors so they are consistent over time and consistent between sensors (Helder, 2008a).

3.2. TM sensors

The TM sensor includes an onboard calibration system called the IC. The IC consists of a black shutter flag, three lamps, a cavity blackbody, and the optical components necessary to get the lamp and blackbody radiance to the focal plane. The lamps are used to calibrate the reflective bands, and the blackbody is used to calibrate the thermal band. Historically, the TM radiometric calibration procedure used the detector's response to the IC to determine radiometric gains and offsets on a scene-by-scene basis. Before launch, the effective radiance of each lamp state for each reflective band's detector was determined such that each detector's response to the internal lamp was compared to its response to an external calibrated source. The reflective band calibration algorithm for in-flight data used a regression of the detector responses against the prelaunch radiances of the eight lamp states. The slope of the regression represented the gain, while the intercept represented the bias. This algorithm assumed that irradiance of the calibration lamps remained constant over time since launch. Any change in response was treated as a change in sensor response, and thus was compensated for during processing. On-orbit data from individual lamps indicated that the lamps were not particularly stable. Because there was no way to validate the lamp radiances once in orbit, the prelaunch measured radiances were the only metrics available for the regression procedure. Recent studies[4] (Thome et al., 1997a, 1997b; Helder et al., 1998; Markham et al., 1998; Teillet et al., 2001, 2004; Chander et al., 2004) indicate that the regression calibration did not actually represent detector gains for most of the mission. However, the regression procedure was used until 2003 to generate L5 TM data products and is still used to generate L4 TM products. The calibration uncertainties of the L4 TM at-sensor

[4] Radiometric performance studies of the TM sensors have also led to a detailed understanding of several image artifacts due to particular sensor characteristics (Helder & Ruggles, 2004a). These artifact corrections (such as Scan-Correlated Shift [SCS], Memory Effect [ME], and Coherent Noise [CN]), along with detector-to-detector normalization (Helder et. al., 2004b), are necessary to maintain the internal consistency of the calibration within a scene.

spectral radiances are ±10%, which was the specified accuracy for the sensor (GSFC specification, 1981).

The L5 TM reflective band calibration procedure was updated in 2003 (Chander & Markham, 2003) to remove the dependence on the changing IC lamps. The new calibration gains implemented on May 5, 2003, for the reflective bands (1–5, 7) were based on lifetime radiometric calibration curves derived from the detectors' responses to the IC, cross-calibration with ETM+, and vicarious measurements (Chander et al., 2004a). The gains were further revised on April 2, 2007, based on the detectors' responses to pseudo-invariant desert sites and cross-calibration with ETM+ (Chander et al., 2007). Although this calibration update applies to all archived and future L5 TM data, the principal improvements in the calibration are for data acquired during the first eight years of the mission (1984–1991), where changes in the sensor gain values are as much as 15%. The radiometric scaling coefficients for Bands 1 and 2 for approximately the first eight years of the mission have also been changed. Along with the revised reflective band radiometric calibration on April 2, 2007, an sensor offset correction of 0.092 W/(m^2 sr μm), or about 0.68 K (at 300 K), was added to all L5 TM thermal band (Band 6) data acquired since April 1999 (Barsi et al., 2007). The L5 TM radiometric calibration uncertainty of the at-sensor spectral radiances is around 5% and is somewhat worse for early years, when the sensor was changing more rapidly, and better for later years (Helder et al., 2008b). The L4 TM reflective bands and the thermal band on both the TM sensors continue to be calibrated using the IC. Further updates to improve the thermal band calibration are being investigated, as is the calibration of the L4 TM.

3.3. ETM+ sensor

The ETM+ sensor has three onboard calibration devices for the reflective bands: a Full Aperture Solar Calibrator (FASC), which is a white painted diffuser panel; a Partial Aperture Solar Calibrator (PASC), which is a set of optics that allows the ETM+ to image the Sun through small holes; and an IC, which consists of two lamps, a blackbody, a shutter, and optics to transfer the energy from the calibration sources to the focal plane. The ETM+ sensor has also been calibrated vicariously using Earth targets such as Railroad Valley (Thome, 2001; Thome et al., 2004) and cross-calibrated with multiple sensors (Teillet et al., 2001, 2006, 2007; Thome et al., 2003; Chander et al., 2004b, 2007b, 2008). The gain trends from the ETM+ sensor are regularly monitored on-orbit using the onboard calibrators and vicarious calibration. The calibration uncertainties of ETM+ at-sensor spectral radiances are ±5%. ETM+ is the most stable of the Landsat sensors, changing by no more than 0.5% per year in its radiometric calibration (Markham et al., 2004b). The ETM+ radiometric calibration procedure uses prelaunch gain coefficients populated in the Calibration Parameter File (CPF). These CPFs, issued quarterly, have both an "effective" and "version" date. The effective date of the CPF must match the acquisition date of

the scene. A CPF version is active until a new CPF for that date period supersedes it. Data can be processed with any version of a CPF; the later versions have more refined parameters, as they reflect more data-rich post-acquisition analysis.

The ETM+ images are acquired in either a low- or high-gain state. The goal of using two gain settings is to maximize the sensors' 8-bit radiometric resolution without saturating the detectors. For all bands, the low-gain dynamic range is approximately 1.5 times the high-gain dynamic range. Therefore, low-gain mode is used to image surfaces with high brightness (higher dynamic range but low sensitivity), and high-gain mode is used to image surfaces with low brightness (lower dynamic range but high sensitivity).

All of the ETM+ acquisitions after May 31, 2003, have an anomaly caused by the failure of the Scan Line Corrector (SLC), which compensated for the forward motion of the spacecraft so that all the scans were aligned parallel with each other. The images with data loss are referred to as SLC-off images, whereas images collected prior to the SLC failure are referred to as SLC-on images (i.e., no data gaps exist). The malfunction of the SLC mirror assembly resulted in the loss of approximately 22% of the normal scene area (Storey et al., 2005). The missing data affects most of the image, with scan gaps varying in width from one pixel or less near the center of the image to 14 pixels along the east and west edges of the image, creating a repeating wedge-shaped pattern along the edges. The middle of the scene, approximately 22 km wide on a Level 1 product, contains very little duplication or data loss. Note that the SLC failure has no impact on the radiometric performance with the valid pixels.

3.4. ALI sensor

The ALI has two onboard radiometric calibration devices: a lamp-based system and a solar-diffuser with variable irradiance controlled by an aperture door. In addition to its onboard calibrators, ALI has the ability to collect lunar and stellar observations for calibration purposes. The ALI radiometric calibration procedure uses a fixed set of detector-by-detector gains established shortly after launch and biases measured shortly after each scene acquisition by closing the ALI's shutter. The calibration uncertainties of the ALI at-sensor spectral radiances are ±5% (Mendenhall & Lencioni, 2002). The ALI sensor is well-behaved and stable, with changes in the response being less than 2% per year even early in the mission, and averaging, at most, slightly more than 1% per year over the full mission (Markham et al., 2006).

4. Conversion to at-sensor spectral radiance (Q_{cal}-to- L_λ)

Calculation of at-sensor spectral radiance is the fundamental step in converting image data from multiple sensors and platforms into a physically meaningful common radiometric scale.

Radiometric calibration of the MSS, TM, ETM+, and ALI sensors involves rescaling the raw digital numbers (Q) transmitted from the satellite to calibrated digital numbers (Q_{cal})[5], which have the same radiometric scaling for all scenes processed on the ground for a specific period.

During radiometric calibration, pixel values (Q) from raw, unprocessed image data are converted to units of absolute spectral radiance using 32-bit floating-point calculations. The absolute radiance values are then scaled to 7-bit (MSS, Q_{calmax} = 127), 8-bit (TM and ETM+, Q_{calmax} = 255), and 16-bit (ALI, Q_{calmax} = 32767) numbers representing Q_{cal} before output to distribution media. Conversion from Q_{cal} in Level 1 products back to at-sensor spectral radiance (L_λ) requires knowledge of the lower and upper limit of the original rescaling factors. The following equation is used to perform the Q_{cal}-to- L_λ conversion for Level 1 products:

$$L_\lambda = \left(\frac{LMAX_\lambda - LMIN_\lambda}{Q_{cal\max} - Q_{cal\min}} \right) (Q_{cal} - Q_{cal\min}) + LMIN_\lambda$$

$$or$$

$$L_\lambda = G_{rescale} \times Q_{cal} + B_{rescale} \qquad (1)$$

$$Where:$$

$$G_{rescale} = \frac{LMAX_\lambda - LMIN_\lambda}{Q_{cal\max} - Q_{cal\min}}$$

$$B_{rescale} = LMIN_\lambda - \left(\frac{LMAX_\lambda - LMIN_\lambda}{Q_{cal\max} - Q_{cal\min}} \right) Q_{cal\min}$$

Where

L_λ = Spectral radiance at the sensor's aperture [W/(m^2 sr μm)]

Q_{cal} = Quantized calibrated pixel value [DN]

Q_{calmin} = Minimum quantized calibrated pixel value corresponding to $LMIN_\lambda$ [DN]

Q_{calmax} = Maximum quantized calibrated pixel value corresponding to $LMAX_\lambda$ [DN]

$LMIN_\lambda$ = Spectral at-sensor radiance that is scaled to Q_{calmin} [W/(m^2 sr μm)]

$LMAX_\lambda$ = Spectral at-sensor radiance that is scaled to Q_{calmax} [W/(m^2 sr μm)]

$G_{rescale}$ = Band-specific rescaling gain factor [(W/(m^2 sr μm))/ DN]

$B_{rescale}$ = Band-specific rescaling bias factor [W/(m^2 sr μm)]

Historically, the MSS and TM calibration information is presented in spectral radiance units of mW/(cm^2 sr μm). To maintain consistency with ETM+ spectral radiance, units of W/(m^2 sr μm) are now used for MSS and TM calibration information. The conversion factor is 1:10 when

[5] These are the DNs that users receive with Level 1 Landsat products.

converting from mW/ (cm^2 sr μm) units to W/ (m^2 sr μm). Tables 2, 3, 4, and 5 summarize the spectral range, post-calibration dynamic ranges[6] ($LMIN_\lambda$ and $LMAX_\lambda$ scaling parameters and the corresponding rescaling gain [$G_{rescale}$]] and rescaling bias [$B_{rescale}$] values), and mean exoatmospheric solar irradiance ($ESUN_\lambda$) for the MSS, TM, ETM+, and ALI sensors, respectively.

Tables 2–5 give the prelaunch "measured" (as-built performance) spectral ranges. These numbers are slightly different from the original filter specification. The center wavelengths are the average of the two spectral range numbers. Figures 1 and 2 show the Relative Spectral Response (RSR) profiles of the Landsat MSS (Markham & Barker, 1983), TM (Markham & Barker, 1986), ETM+ (Handbook[1]), and ALI (Mendenhall & Parker, 1999) sensors measured during prelaunch characterization. The ETM+ spectral bands were designed to mimic the standard TM spectral bands 1–7. The ALI bands were designed to mimic the six standard ETM+ solar reflective spectral bands 1–5, and 7; three new bands, 1p, 4p, and 5p, were added to more effectively address atmospheric interference effects and specific applications. The ALI band numbering corresponds with the ETM+ spectral bands. Bands not present on the ETM+ sensor are given the "p," or prime, designation. MSS spectral bands are significantly different from TM and ETM+ spectral bands.

The post-calibration dynamic ranges are band-specific rescaling factors typically provided in the Level 1 product header file. Over the life of the Landsat sensors, occasional changes have occurred in the post-calibration dynamic range. Future changes are anticipated, especially in the MSS and TM data, because of the possible adjustment of the calibration constants based on comparisons to absolute radiometric measurements made on the ground. In some cases, the header file may have different rescaling factors than provided in the table included here. In these cases, the user should use the header file information that comes with the product.

Two processing systems will continue to generate Landsat data products: the Level 1 Product Generation System (LPGS) and the National Land Archive Production System (NLAPS). Starting December 8, 2008, all L7 ETM+ and L5 TM (except Thematic Mapper-Archive [TM-A][7] products) standard Level 1 products are processed through the LPGS, and all L4 TM and MSS

[6] The post-calibration dynamic ranges summarized in Tables 2–5 are only applicable to Landsat data processed and distributed by the USGS EROS Center. The IGSs may process the data differently, and these rescaling factors may not be applicable. "Special collections," such as the Multi-Resolution Land Characteristics Consortium (MRLC) or Global Land Survey (GLS), may have a different processing history, so the user needs to verify the respective product header information.

[7] A small number of TM scenes were archived as radiometrically corrected products known as TM-A data. The TM-A data are archived on a scene-by-scene basis (instead of intervals). The L4 and L5 TM-A scenes will continue to be processed using NLAPS (with Q_{calmin} =0), which attempts to uncalibrate the previously applied calibration and generates the product using updated calibration procedures. Note that approximately 80 L4 TM and approximately 13,300 L5 TM scenes are archived as TM-A data, with acquisition dates ranging between Sept.1982 and Aug. 1990.

standard Level 1 products are processed through the NLAPS. The Landsat Program is working toward transitioning the processing of all Landsat data to LPGS (Kline, personal communication). In mid-2009, the processing of L4 TM data will transition from NLAPS to LPGS. The scenes processed using LPGS include a header file (.MTL), which lists the $LMIN_\lambda$ and $LMAX_\lambda$ values but not the rescaling gain and bias numbers. The scenes processed using NLAPS include a processing history work order report (.WO), which lists the rescaling gain and bias numbers but not the $LMIN_\lambda$ and $LMAX_\lambda$.

The sensitivity of the detector changes over time, causing a change in the detector gain applied during radiometric calibration. However, the numbers presented in Tables 2–5 are the rescaling factors, which are the post-calibration dynamic ranges. The $LMIN_\lambda$ and $LMAX_\lambda$ are a representation of how the output Landsat Level 1 data products are scaled in at-sensor radiance units. Generally, there is no need to change the $LMIN_\lambda$ or $LMAX_\lambda$ unless something changes drastically on the sensor. Thus, there is no time dependence for any of the rescaling factors in Tables 2–5.

5. Conversion to TOA reflectance (L_λ-to-ρ_P)

A reduction in scene-to-scene variability can be achieved by converting the at-sensor spectral radiance to exoatmospheric TOA reflectance, also known as in-band planetary albedo. When comparing images from different sensors, there are three advantages to using TOA reflectance instead of at-sensor spectral radiance. First, it removes the cosine effect of different solar zenith angles due to the time difference between data acquisitions. Second, TOA reflectance compensates for different values of the exoatmospheric solar irradiance arising from spectral band differences. Third, the TOA reflectance corrects for the variation in the Earth-Sun distance between different data acquisition dates. These variations can be significant geographically and temporally. The TOA reflectance of the Earth is computed according to the equation:

$$\rho_\lambda = \frac{\pi \cdot L_\lambda \cdot d^2}{ESUN_\lambda \cdot \cos\theta_s} \quad (2)$$

where

ρ_λ = Planetary TOA reflectance [unitless]

π = Mathematical constant approximately equal to 3.14159 [unitless]

L_λ =Spectral radiance at the sensor's aperture [W/(m^2 sr μm)]

d = Earth-Sun distance [astronomical units]

$ESUN_\lambda$ = Mean exoatmospheric solar irradiance [W/(m^2 μm)]

θ_s = Solar zenith angle [degrees[8]]

Note that the cosine of the solar zenith angle is equal to the sine of the solar elevation angle. The solar elevation angle at the Landsat scene center is typically stored in the Level 1 product header file (.MTL or .WO) or retrieved from the USGS EarthExplorer or GloVis online interfaces under the respective scene metadata (these web sites also contain the acquisition time in hours, minutes, and seconds). The reflectance calculation requires the Earth-Sun distance (d). Table 6 presents d in astronomical units throughout a year generated using the Jet Propulsion Laboratory (JPL) Ephemeris[9] (DE405) data. The d numbers are also tabulated in the Nautical Almanac.

The last column of Tables 2–5 summarizes solar exoatmospheric spectral irradiances ($ESUN_\lambda$) for the MSS, TM, ETM+, and ALI sensors using the Thuillier solar spectrum (Thuillier et al., 2003). The Committee on Earth Observation Satellites (CEOS) Working Group on Calibration and Validation (WGCV) recommends[10] using this spectrum for applications in optical-based Earth Observation that use an exoatmospheric solar irradiance spectrum. The Thuillier spectrum is believed to be the most accurate and an improvement over the other solar spectrum. Note that the CHKUR solar spectrum in MODTRAN 4.0 (Air Force Laboratory, 1998) was used previously for ETM+ (Handbook[1]) and TM (Chander & Markham, 2003), whereas the Neckel and Lab (Neckel & Lab, 1984) and Iqbal (Iqbal, 1983) solar spectrums were used for MSS and TM solar irradiance values (Markham & Barker, 1986). The primary differences occur in Bands 5 and 7. For comparisons to other sensors, users need to verify that the same solar spectrum is used for all sensors.

6. Conversion to at-sensor brightness temperature (L_λ-to- T)

The thermal band data (Band 6 on TM and ETM+) can be converted from at-sensor spectral radiance to effective at-sensor brightness temperature. The at-sensor brightness temperature assumes that the Earth's surface is a black body (i.e., spectral emissivity is 1), and includes atmospheric effects (absorption and emissions along path). The at-sensor temperature uses the prelaunch calibration constants given in Table 7. The conversion formula from the at-sensor's spectral radiance to at-sensor brightness temperature is:

[8] Note that Excel, Matlab, C, and many other software applications use radians, not degrees, to perform calculations. The conversion from degrees to radians is a multiplication factor of pi/180.

[9] http://ssd.jpl.nasa.gov/?horizons

[10] CEOS-recommended solar irradiance spectrum, http://wgcv.ceos.org

$$T = \frac{K2}{\ln\left(\frac{K1}{L_\lambda} + 1\right)} \tag{3}$$

where:

T = Effective at-sensor brightness temperature [K]

K2 = Calibration constant 2 [K]

K1 = Calibration constant 1 [W/(m^2 sr μm)]

L_λ = Spectral radiance at the sensor's aperture [W/(m^2 sr μm)]

ln = Natural logarithm

The ETM+ Level 1 product has two thermal bands, one acquired using a low gain setting (often referred to as Band 6L; useful temperature range of 130–350 K) and the other using a high gain setting (often referred to as Band 6H; useful temperature range of 240–320 K). The noise equivalent change in temperature (NEΔT) at 280 K for ETM+ high gain is 0.22 and for low gain is 0.28. The TM Level 1 product has only one thermal band (there is no gain setting on the TM sensor), and the thermal band images have a useful temperature range of 200–340 K. The NEΔT at 280 K for L5 TM is 0.17–0.30 (Barsi et al., 2003).

7. Conclusion

This paper provides equations and rescaling factors for converting Landsat calibrated DNs to absolute units of at-sensor spectral radiance, TOA reflectance, and at-sensor brightness temperature. It tabulates the necessary constants for the MSS, TM, ETM+, and ALI sensors in a coherent manner using the same units and definitions. This paper forms a needed guide for Landsat data users who now have access to the entire Landsat archive at no cost. Studies are ongoing to evaluate the MSS calibration consistency and provide post-calibration adjustments of the MSS sensors so they are consistent over time and consistent between sensors. Further updates to improve the TM and ETM+ thermal band calibration are being investigated, as is the calibration of the L4 TM.

Acknowledgments

The authors acknowledge the support of David Aaron (SDSU) for digitizing the spectral responses for the MSS sensors and Julia Barsi (SSAI) for generating the Earth-Sun distance. Special thanks are extended to a number of colleagues for reviewing drafts of this manuscript. The anonymous reviewers' comments were particularly valuable and their efforts are greatly appreciated. Any use of trade, product, or firm names is for descriptive purposes only and does not imply endorsement by the U.S. Government.

References

Air Force Research Laboratory. (1998). Modtran Users Manual, Versions 3.7 and 4.0, Hanscom Air Force Base, MA.

Barsi, J.A., Schott, J.R., Palluconi, F.D., Helder, D.L., Hook, S.J., Markham, B.L., Chander, G., & O'Donnell, E.M. (2003). Landsat TM and ETM+ thermal band calibration. *Can. J. Remote Sensing*, 29(2), 141–153.

Barsi, J.A., Hook, S.J., Schott, J.R., Raqueno, N.G., & Markham, B.L. (2007). Landsat-5 Thematic Mapper thermal band calibration update. *IEEE Transactions on Geoscience and Remote Sensing*, *44*, 552–555.

Chander, G. & Markham, B.L. (2003). Revised Landsat-5 TM radiometric calibration procedures, and post-calibration dynamic ranges. *IEEE Transactions on Geoscience and Remote Sensing*, *41***,** 2674–2677.

Chander, G., Helder, D.L., Markham, B.L., Dewald, J., Kaita, E., Thome, K.J., Micijevic, E., & Ruggles, T. (2004a). Landsat 5 TM on-orbit absolute radiometric performance. *IEEE Transactions on Geoscience and Remote Sensing*, *42***,** 2747–2760.

Chander, G., Meyer, D.J., & Helder, D.L. (2004b). Cross-Calibration of the Landsat-7 ETM+ and EO-1 ALI sensors. *IEEE Transactions on Geoscience and Remote Sensing*, *42*(12), 2821–2831.

Chander, G., Markham, B.L., & Barsi, J.A. (2007a). Revised Landsat 5 Thematic Mapper radiometric calibration. *IEEE Transactions on Geoscience and Remote Sensing*, *44*, 490–494.

Chander, G., Angal, A., Choi, T., Meyer, D.J., Xiong, X., & Teillet, P.M. (2007b). Cross-calibration of the Terra MODIS, Landsat-7 ETM+ and EO-1 ALI sensors using near simultaneous surface observation over Railroad Valley Playa, Nevada test site. In J. J. Butler, & J. Xiong (Eds.), *Proceedings of SPIE Conference 6677 on Earth Observing Systems XII, SPIE,* Vol. 6677 (pp. 66770Y: 1-12). San Diego, CA.

Chander, G., Coan, M.J., & Scaramuzza, P.L. (2008). Evaluation and Comparison of the IRS-P6 and the Landsat Sensors. *IEEE Transactions on Geoscience and Remote Sensing*, *46*(1), 209–221.

Cohen, W.B., & Goward, S.N. (2004). Landsat's role in ecological applications of remote sensing. *BioScience*, 54 (6), 535-545

Fuller, R.M., Groom, G.B., Jones, A.R. (1994). The land cover map of Great Britain: an automated classification of Landsat Thematic Mapper data," *Photogrammetric Engineering & Remote Sensing*, vol. 60, pp. 553–562.

Goward, S.N., & Williams, D.L. (1997). Landsat and Earth Systems Science: Development of terrestrial monitoring. *Photogrammetric Engineering and Remote Sensing*, 63 (7), 887-900.

Goward, S., Irons, J., Franks, S., Arvidson, T., Williams, D., Faundeen, J. (2006). Historical record of landsat global coverage: Mission operations, NSLRSDA, and international cooperator stations. *Photogrammetric Engineering and Remote Sensing*, vol. 72, pp. 1155–1169.

GSFC Specification for the Thematic Mapper System and Associated Test Equipment. (Rev C., January 1981) GSFC 400-8-D-210C, NASA, Goddard Space Flight Center, Greenbelt, MD.

Helder, D.L (1993). MSS Radiometric Calibration Handbook. *Report to the U.S. Geological Survey (USGS) Earth Resources Observation and Science (EROS) Center.*

Helder, D.L., Boncyk, W.C., Morfitt, R. (1998). Absolute calibration of the Landsat Thematic Mapper using the internal calibrator. *Proc. IGARSS*, Seattle, WA, 1998, pp. 2716–2718.

Helder, D.L, & Ruggles, T.A. (2004a). Landsat Thematic Mapper reflectiveband radiometric artifacts. *IEEE Transactions on Geoscience and Remote Sensing*, *44*, 2704–2716.

Helder, D.L, Ruggles, T.A., Dewald, J.D., Madhavan, S. (2004b). Landsat-5 Thematic Mapper reflective-band radiometric stability. *IEEE Transactions on Geoscience and Remote Sensing*, *44*, 2704–2716.

Helder, D.L (2008a). Consistent Radiometric Calibration of the Historical Landsat Archive. *Proceedings of PECORA*. Denver, Colorado

Helder, D.L., Markham, B. L., Thome, K. J., Barsi, J. A., Chander, G., & Malla R. (2008 b). Updated radiometric calibration for the Landsat 5 Thematic Mapper reflective bands. *IEEE Transactions on Geoscience and Remote Sensing*, *46*(10), 3309–3325.

Iqbal, M., 1983, Introduction to Solar Radiation (New York: Academic Press).

Markham, B.L., & Barker, J.L. (1983). Spectral characterization of the Landsat-4 MSS sensors. *Photogrammetric Engineering and Remote Sensing*. *49*(6), 811-833.

Markham, B. L., & Barker, J.L., (1985). Spectral characterization of the LANDSAT Thematic Mapper sensors', *International Journal of Remote Sensing*, 6:(5) 697 – 716.

Markham, B.L., & Barker, J.L. (1986). Landsat MSS and TM post-calibration dynamic ranges, exoatmospheric reflectances and at-satellite temperatures. *Earth Observation Satellite Co.,* Lanham, MD, Landsat Tech. Note 1.

Markham, B.L., & Barker, J.L. (1987). Radiometric properties of U.S. processed Landsat MSS Data. *Remote Sensing of Environment*, *22,* 39–71.

Markham, B.L., Seiferth, J.C., Smid, J., Barker, J.L (1998). Lifetime responsivity behavior of the Landsat-5 Thematic Mapper. *Proceedings of SPIE Conference 3427 on Earth Observing Systems, SPIE,* Vol. 3427 (pp. 420-431). San Diego, CA.

Markham, B.L., Chander, G., Morfitt, R., Hollaren, D., Mendenhall, J.F., & Ong, L. (2004a). Radiometric processing and calibration of EO-1 Advanced Land Imager data. *Proceedings of PECORA 16 "Global Priorities in Land Remote Sensing"*. Sioux Falls, South Dakota.

Markham, B.L, Thome, K., Barsi, J., Kaita, E., Helder, D., Barker, J., & Scaramuzza, P. (2004b). Landsat-7 ETM+ On-Orbit reflective-band radiometric stability and absolute calibration. *IEEE Transactions on Geoscience and Remote Sensing*, *42*, 2810–2820.

Markham, B.L., Ong, L., Barsi, J.A., Mendenhall, J.A., Lencioni D.E., Helder, D.L., Hollaren, D.H., Morfitt, R.M. (2006). Radiometric calibration stability of the EO-1 Advanced Land Imager: 5 Years on-orbit. In R. Meynart, S. P. Neeck, H. Shimoda (Eds.), *Proceedings of SPIE Conference 6361 on Sensors, Systems, and Next-Generation Satellites X, SPIE,* Vol. 6361 (pp. 66770U: 1-12). San Diego, CA.

Masek, J. G., Vermote, Huang, C., Wolfe, R., Cohen W., Hall, F., Kutler, J., Nelson, P. (2008). North American forest disturbance mapped from a decadal Landsat record," *Remote Sensing of Environment,* 112, 2914–2926.

Mendenhall, J. A., & Parker, A. C. (1999). Spectral calibration of the EO-1 Advanced Land Imager. *Proceedings of SPIE Conference 3750 on Earth Observing Systems IV*, SPIE, Vol. 3750, (pp. 109-116), Denver, Colorado.

Mendenhall, J.A., & Lencioni, D.E. (2002). EO-1 Advanced Land Imager On-Orbit Radiometric Calibration, *International Geoscience and Remote Sensing Symposium*. Toronto, Canada.

Nautical Almanac Office. The Nautical Almanac for the Year (United States Naval Observatory) (Washington, DC: U.S. Government Printing Office).

Neckel, H., and Labs, D. (1984). The solar radiation between 3300 and 12500 A. Sol. Phys., 90,205.

Roy, D., Borak, J, Devadiga, S., Wolfe, R., Zheng, M., Descloitres, J. (2002). The MODIS land product quality assessment approach, *Remote Sensing of Environment,* 83:62-76.

Special Issue on Landsat 4 (1984). *IEEE Transactions on Geoscience and Remote Sensing*, GE-22 (3) 160, 51(9). Guest Editor: Solomonson, V.V.

Special Issue on Landsat Image Data Quality Analysis (LIDQA) (1985). *Photogrammetric Engineering and Remote Sensing*, 51(9). Guest Editors: Markham, B. L., and Barker, J.L.

Special Issue on 25th Anniversary of Landsat (1997). *Photogrammetric Engineering and Remote Sensing*, 63(7). Guest Editor: Salomonson, V.V.

Special Issue on Landsat 7. (2001). *Remote Sensing of Environment*, 78 (1–2), 1–220. Guest Editors: Goward, S.N., and Masek, J.G.

Special Issue on Synergistic Utilization of Landsat 7. (2003). *Canadian Journal of Remote Sensing*, 29 (2), 141–297. Guest Editor: Teillet, P.M.

Special Issue on Landsat Sensor Performance Characterization. (2004). *IEEE Transactions on Geoscience and Remote Sensing*, 42(12) 2687–2855. Guest Editors: Markham, B.L., Storey, J.C., Crawford, M.M., Goodenough, D.G., Irons, J.R.

Special Issue on Landsat Operations: Past, Present and Future. (2006). *Photogrammetric Engineering and Remote Sensing*, 72(10). Guest Editors: Williams, D.L, Goward, S.N., Arvidson, T.

Storey, J.C, Scaramuzza, P., and Schmidt, G. (2005). Landsat 7 scan line corrector-off gap filled product development. *PECORA 16 Conference Proceedings, Sioux Falls, South Dakota*, 23–27.

Teillet, P.M, Barker, J.L, Markham, B.L, Irish, R.R, Fedosejeves, G., & Storey, J.C. (2001). Radiometric Cross-Calibration of the Landsat-7 ETM+ and Landsat-5 TM Sensors Based on Tandem Data Sets. *Remote Sensing of Environment, 78*(1–2), 39–54.

Teillet, P. M., Helder, D. L., Ruggles, T. A., Landry, R., Ahern, F. J., Higgs, N. J., et al. (2004). A Definitive Calibration Record for the Landsat-5 Thematic Mapper Anchored to the Landsat-7 Radiometric Scale. *Canadian Journal of Remote Sensing,* 30(4), 631−643.

Teillet, P. M., Markham, B. L., & Irish, R. R. (2006). Landsat cross-calibration based on near simultaneous imaging of common ground targets. *Remote Sensing of Environment,* 102(3–4), 264−270.

Teillet, P.M., Fedosejevs, G., Thome, K.J., & Barker, J.L. (2007). Impacts of spectral band difference effects on radiometric cross-calibration between satellite sensors in the solar-reflective spectral domain. *Remote Sensing of Environment,* 110, 393–409.

Thome, K.J., Markham, B.L., Barker, J.L., Slater, P.L., Biggar, S. (1997a). Radiometric calibration of Landsat. *Photogramm. Eng. Remote Sens.,* vol. 63, pp. 853–858.

Thome, K. J., Crowther, B. G., & Biggar, S. F. (1997b). Reflectance- and Irradiance-Based Calibration of Landsat-5 Thematic Mapper. *Canadian Journal of Remote Sensing,* 23, 309−317.

Thome, K.J. (2001). Absolute Radiometric Calibration of Landsat 7 ETM+ Using the Reflectance-Based Method. *Remote Sensing of Environment, 78*(1–2), 27−38.

Thome, K. J., Biggar, S. F., & Wisniewski, W. (2003). Cross Comparison of EO-1 Sensors and Other Earth Resources Sensors to Landsat-7 ETM+ Using Railroad Valley Playa. *IEEE Transactions on Geoscience and Remote Sensing,* 41, 1180−1188.

Thome, K.J., Helder, D.L., Aaron, D.A., & Dewald, J. (2004). Landsat 5 TM and Landsat-7 ETM+ Absolute Radiometric Calibration using Reflectance Based Method. *IEEE Transactions on Geoscience and Remote Sensing*, *42*(12), 2777− 2785.

Thuillier, G., Herse, M., Labs, S., Foujols, T., Peetermans, W., Gillotay, D., Simon, P.C., Mandel, H. (2003). The Solar Spectral Irradiance from 200 to 2400nm as Measured by SOLSPEC Spectrometer from the ATLAS 123 and EURECA Missions*. Solar Physics, Solar Physics,* v. 214, Issue 1, p. 1-22.

Townshend, J.R.G., Bell, V., Desch, A.C., Havlicek, C., Justice, C.O., Lawrence, W.E., Skole, D., Chomentowski, W.W., Moore, B., Salas, W., Tucjer, C.J. (1995). The NASA Landsat Pathfinder Humid Tropical Deforestation Project. *In Proceedings Land Satellite Information in the Next Decade, ASPRS Conference*, (pp. 76-87). Vienna, Virginia

Vogelmann, J.E., Howard, S.M., Yang, L., Larson, C.R., Wylie, B.K., Van Driel, J.N. (2001). Completion of the 1990's National Land Cover Data Set for the conterminous United States," *Photogrammetric Engineering and Remote Sensing*, vol. 67, pp. 650–662.

Woodcock, C.E., Macomber, S.A., Pax-Lenney, M., Cohen, W.C. (2006). Monitoring large areas for forest change using Landsat: Generalization across space, time and Landsat sensors. *Remote Sensing of Environment*, 78, 194-203.

Woodcock, C.E., Allen, A.A., Anderson, M., Belward, A.S., Bindschadler, R., Cohen, W.B., Gao, F., Goward, S.N., Helder, D., Helmer, E., Nemani, R., Oreapoulos, L., Schott, J., Thenkabail, P.S., Vermote, E.F., Vogelmann, J., Wulder, M.A., Wynne, R. , 2008, Free access to Landsat imagery, *Science,* 320:1011.

Wulder, M.A., White, J.C., Goward, S.N., Masek, J.G., Irons, J.R., Herold, M., Cohen, W.B., Loveland, T.R., Woodcock, C. E. (2008). Landsat continuity: Issues and opportunities for land cover monitoring. *Remote Sensing of Environment*, 112, 955-969.

Table 1
Landsat satellites launch dates

Satellite	Sensors	Launch Date	Decommission	Altitude	Inclination	Period	Repeat Cycle	Crossing
				km	degrees	min	days	time (a.m.)
Landsat 1	MSS and RBV	July 23, 1972	January 7, 1978	920	99.20	103.34	18	9:30
Landsat 2	MSS and RBV	January 22, 1975	February 25, 1982	920	99.20	103.34	18	9:30
Landsat 3	MSS and RBV	March 5, 1978	March 31, 1983	920	99.20	103.34	18	9:30
Landsat 4	MSS and TM	July 16, 1982	June 30, 2001	705	98.20	98.20	16	9:45
Landsat 5	MSS and TM	March 1, 1984	Operational	705	98.20	98.20	16	9:45
Landsat 6	ETM	October 5, 1993	Did not achieve orbit					
Landsat 7	ETM+	April 15, 1999	Operational	705	98.20	98.20	16	10:00
EO-1	ALI	November 21, 2000	Operational	705	98.20	98.20	16	10:01

Table 2
MSS spectral range, post-calibration dynamic ranges, and mean exoatmospheric solar irradiance ($ESUN_\lambda$)

MSS Sensors (Q_{calmin} = 0 and Q_{calmax} = 127)							
Band	**Spectral Range**	**Center Wavelength**	**$LMIN_\lambda$**	**$LMAX_\lambda$**	**$G_{rescale}$**	**$B_{rescale}$**	**$ESUN_\lambda$**
Units	**µm**		**W/(m^2 sr µm)**		**(W/m^2 sr µm)/DN**	**W/(m^2 sr µm)**	**W/(m^2.µm)**
L1 MSS (NLAPS)							
1	0.499 – 0.597	0.548	0	248	1.952760	0	1823
2	0.603 – 0.701	0.652	0	200	1.574800	0	1559
3	0.694 – 0.800	0.747	0	176	1.385830	0	1276
4	0.810 – 0.989	0.900	0	153	1.204720	0	880.1
L2 MSS (NLAPS)							
1	0.497 – 0.598	0.548	8	263	2.007870	8	1829
2	0.607 – 0.710	0.659	6	176	1.338580	6	1539
3	0.697 – 0.802	0.750	6	152	1.149610	6	1268
4	0.807 – 0.990	0.899	3.66667	130.333	0.997373	3.66667	886.6
L3 MSS (NLAPS)							
1	0.497 – 0.593	0.545	4	259	2.007870	4	1839
2	0.606 – 0.705	0.656	3	179	1.385830	3	1555
3	0.693 – 0.793	0.743	3	149	1.149610	3	1291
4	0.812 – 0.979	0.896	1	128	1.000000	1	887.9
L4 MSS (NLAPS)							
1	0.495 – 0.605	0.550	4	238	1.842520	4	1827
2	0.603 – 0.696	0.650	4	164	1.259840	4	1569
3	0.701 – 0.813	0.757	5	142	1.078740	5	1260
4	0.808 – 1.023	0.916	4	116	0.881890	4	866.4
L5 MSS (NLAPS)							
1	0.497 – 0.607	0.552	3	268	2.086610	3	1824
2	0.603 – 0.697	0.650	3	179	1.385830	3	1570
3	0.704 – 0.814	0.759	5	148	1.125980	5	1249
4	0.809 – 1.036	0.923	3	123	0.944882	3	853.4

Note 1: In some cases, the header file may have different rescaling factors than provided here. In these cases, the user should use the header file information that comes with the product. Tables 1 (Markham & Barker, 1986, 1987) provide a summary of the band-specific $LMIN_\lambda$ and $LMAX_\lambda$ rescaling factors that have been used at different times and by different systems for the ground processing of MSS data.

Table 3
TM spectral range, post-calibration dynamic ranges, and mean exoatmospheric solar irradiance ($ESUN_\lambda$)

TM Sensors (Q_{calmin} = 1 and Q_{calmax} = 255)							
Band	**Spectral Range**	**Center Wavelength**	**$LMIN_\lambda$**	**$LMAX_\lambda$**	**$G_{rescale}$**	**$B_{rescale}$**	**$ESUN_\lambda$**
Units	**µm**		**W/(m² sr µm)**		**(W/m² sr µm)/DN**	**W/(m² sr µm)**	**W/(m².µm)**
L4 TM (NLAPS)							
1	0.452 – 0.518	0.485	-1.52	152.10	0.602431	-1.52	1983
2	0.529 – 0.609	0.569	-2.84	296.81	1.175098	-2.84	1795
3	0.624 – 0.693	0.659	-1.17	204.30	0.805765	-1.17	1539
4	0.776 – 0.905	0.841	-1.51	206.20	0.814549	-1.51	1028
5	1.568 – 1.784	1.676	-0.37	27.19	0.108078	-0.37	219.8
6	10.42 – 11.66	11.040	1.2378	15.3032	0.055158	1.2378	N/A
7	2.097 – 2.347	2.222	-0.15	14.38	0.056980	-0.15	83.49
L4 TM (LPGS)							
1	0.452 – 0.518	0.485	-1.52	163	0.647717	-2.17	1983
			-1.52	171	0.679213	-2.20	
2	0.529 – 0.609	0.569	-2.84	336	1.334016	-4.17	1795
3	0.624 – 0.693	0.659	-1.17	254	1.004606	-2.17	1539
4	0.776 – 0.905	0.841	-1.51	221	0.876024	-2.39	1028
5	1.568 – 1.784	1.676	-0.37	31.4	0.125079	-0.50	219.8
6	10.42 – 11.66	11.040	1.2378	15.3032	0.055376	1.2378	N/A
7	2.097 – 2.347	2.222	-0.15	16.6	0.065945	-0.22	83.49
L5 TM (LPGS)							
1	0.452 – 0.518	0.485	-1.52	169	0.671339	-2.19	1983
			-1.52	193	0.765827	-2.29	
2	0.528 – 0.609	0.569	-2.84	333	1.322205	-4.16	1796
			-2.84	365	1.448189	-4.29	
3	0.626 – 0.693	0.660	-1.17	264	1.043976	-2.21	1536
4	0.776 – 0.904	0.840	-1.51	221	0.876024	-2.39	1031
5	1.567 – 1.784	1.676	-0.37	30.2	0.120354	-0.49	220.0
6	10.45 – 12.42	11.435	1.2378	15.3032	0.055376	1.18	N/A
7	2.097 – 2.349	2.223	-0.15	16.5	0.065551	-0.22	83.44

Note 1: The Q_{calmin} = 0 for data processed using NLAPS. The Q_{calmin} = 1 for data processed using LPGS.

Note 2: The $LMIN_\lambda$ is typically set to a small negative number, so a "zero radiance" target will be scaled to a small positive DN value, even in the presence of sensor noise (typically 1 DN or less [1 sigma]). This value is usually not changed throughout the mission.

Note 3: In mid-2009, the processing of L4 TM data will transition from NLAPS to LPGS. NLAPS used IC-based calibration. The L4 TM data processed by LPGS will be radiometrically calibrated using a new lifetime gain model procedure and revised calibration parameters. Use the header file information that comes with the product and the above rescaling factors will not be applicable. The numbers highlighted in grey are the revised ($LMAX_\lambda$ = 163.0) post-calibration dynamic ranges for L4 TM Band 1 data acquired between July 16, 1982 (launch), and August 23, 1986.

Note 4: The radiometric scaling coefficients for L5 TM Bands 1 and 2 for approximately the first eight years (1984–1991) of the mission were changed to optimize the dynamic range and better preserve the sensitivity of the early mission data. The numbers highlighted in grey are the revised ($LMAX_\lambda$ = 169.0, 333.0) post-calibration dynamic ranges for L5 TM Band 1 & 2 data acquired between March 1, 1984 (launch), and December 31, 1991 (Chander et al., 2007a).

Table 4
ETM+ spectral range, post-calibration dynamic ranges, and mean exoatmospheric solar irradiance ($ESUN_\lambda$)

L7 ETM+ Sensor (Q_{calmin} = 1 and Q_{calmax} = 255)							
Low Gain (LPGS)							
Band	Spectral Range	Center Wavelength	$LMIN_\lambda$	$LMAX_\lambda$	$G_{rescale}$	$B_{rescale}$	$ESUN_\lambda$
Units	μm		W/(m² sr μm)		(W/m² sr μm)/DN	W/(m² sr μm)	W/(m².μm)
1	0.452 – 0.514	0.483	-6.2	293.7	1.180709	-7.38	1997
2	0.519 – 0.601	0.560	-6.4	300.9	1.209843	-7.61	1812
3	0.631 – 0.692	0.662	-5.0	234.4	0.942520	-5.94	1533
4	0.772 – 0.898	0.835	-5.1	241.1	0.969291	-6.07	1039
5	1.547 – 1.748	1.648	-1.0	47.57	0.191220	-1.19	230.8
6	10.31 – 12.36	11.335	0.0	17.04	0.067087	-0.07	N/A
7	2.065 – 2.346	2.206	-0.35	16.54	0.066496	-0.42	84.90
PAN	0.515 – 0.896	0.706	-4.7	243.1	0.975591	-5.68	1362
High Gain (LPGS)							
Band	Spectral Range	Center Wavelength	$LMIN_\lambda$	$LMAX_\lambda$	$G_{rescale}$	$B_{rescale}$	$ESUN_\lambda$
Units	μm		W/(m² sr μm)		(W/m² sr μm)/DN	W/(m² sr μm)	W/(m².μm)
1	0.452 – 0.514	0.483	-6.2	191.6	0.778740	-6.98	1997
2	0.519 – 0.601	0.560	-6.4	196.5	0.798819	-7.20	1812
3	0.631 – 0.692	0.662	-5.0	152.9	0.621654	-5.62	1533
4	0.772 – 0.898	0.835	-5.1	157.4	0.639764	-5.74	1039
5	1.547 – 1.748	1.648	-1.0	31.06	0.126220	-1.13	230.8
6	10.31 – 12.36	11.335	3.2	12.65	0.037205	3.16	N/A
7	2.065 – 2.346	2.206	-0.35	10.80	0.043898	-0.39	84.90
PAN	0.515 – 0.896	0.706	-4.7	158.3	0.641732	-5.34	1362

Table 5
ALI spectral range, post-calibration dynamic ranges, and mean exoatmospheric solar irradiance ($ESUN_\lambda$). All EO-1 ALI standard Level 1 products are processed through the EO-1 Product Generation System (EPGS).

EO-1 ALI Sensor (Q_{calmin} = 1 and Q_{calmax} = 32767)							
Band	**Spectral Range**	**Center Wavelength**	**$LMIN_\lambda$**	**$LMAX_\lambda$**	**$G_{rescale}$**	**$B_{rescale}$**	**$ESUN_\lambda$**
Units	**µm**		**W/(m² sr µm)**		**(W/m² sr µm)/DN**	**W/(m² sr µm)**	**W/(m².µm)**
PAN	0.480 – 0.690	0.585	-2.18	784.2	0.024	-2.2	1724
1P	0.433 – 0.453	0.443	-3.36	1471	0.045	-3.4	1857
1	0.450 – 0.515	0.483	-4.36	1405	0.043	-4.4	1996
2	0.525 – 0.605	0.565	-1.87	915.5	0.028	-1.9	1807
3	0.633 – 0.690	0.662	-1.28	588.5	0.018	-1.3	1536
4	0.775 – 0.805	0.790	-0.84	359.6	0.011	-0.85	1145
4P	0.845 – 0.890	0.868	-0.641	297.5	0.0091	-0.65	955.8
5P	1.200 – 1.300	1.250	-1.29	270.7	0.0083	-1.3	452.3
5	1.550 – 1.750	1.650	-0.597	91.14	0.0028	-0.6	235.1
7	2.080 – 2.350	2.215	-0.209	29.61	0.00091	-0.21	82.38

Table 6
Earth-Sun distance (d) in astronomical units for Day of the Year (DOY)

DOY	d	DOY	d	DOY	d	DOY	d	DOY	d	DOY	d
1	0.98331	61	0.99108	121	1.00756	181	1.01665	241	1.00992	301	0.99359
2	0.98330	62	0.99133	122	1.00781	182	1.01667	242	1.00969	302	0.99332
3	0.98330	63	0.99158	123	1.00806	183	1.01668	243	1.00946	303	0.99306
4	0.98330	64	0.99183	124	1.00831	184	1.01670	244	1.00922	304	0.99279
5	0.98330	65	0.99208	125	1.00856	185	1.01670	245	1.00898	305	0.99253
6	0.98332	66	0.99234	126	1.00880	186	1.01670	246	1.00874	306	0.99228
7	0.98333	67	0.99260	127	1.00904	187	1.01670	247	1.00850	307	0.99202
8	0.98335	68	0.99286	128	1.00928	188	1.01669	248	1.00825	308	0.99177
9	0.98338	69	0.99312	129	1.00952	189	1.01668	249	1.00800	309	0.99152
10	0.98341	70	0.99339	130	1.00975	190	1.01666	250	1.00775	310	0.99127
11	0.98345	71	0.99365	131	1.00998	191	1.01664	251	1.00750	311	0.99102
12	0.98349	72	0.99392	132	1.01020	192	1.01661	252	1.00724	312	0.99078
13	0.98354	73	0.99419	133	1.01043	193	1.01658	253	1.00698	313	0.99054
14	0.98359	74	0.99446	134	1.01065	194	1.01655	254	1.00672	314	0.99030
15	0.98365	75	0.99474	135	1.01087	195	1.01650	255	1.00646	315	0.99007
16	0.98371	76	0.99501	136	1.01108	196	1.01646	256	1.00620	316	0.98983
17	0.98378	77	0.99529	137	1.01129	197	1.01641	257	1.00593	317	0.98961
18	0.98385	78	0.99556	138	1.01150	198	1.01635	258	1.00566	318	0.98938
19	0.98393	79	0.99584	139	1.01170	199	1.01629	259	1.00539	319	0.98916
20	0.98401	80	0.99612	140	1.01191	200	1.01623	260	1.00512	320	0.98894
21	0.98410	81	0.99640	141	1.01210	201	1.01616	261	1.00485	321	0.98872
22	0.98419	82	0.99669	142	1.01230	202	1.01609	262	1.00457	322	0.98851
23	0.98428	83	0.99697	143	1.01249	203	1.01601	263	1.00430	323	0.98830
24	0.98439	84	0.99725	144	1.01267	204	1.01592	264	1.00402	324	0.98809
25	0.98449	85	0.99754	145	1.01286	205	1.01584	265	1.00374	325	0.98789
26	0.98460	86	0.99782	146	1.01304	206	1.01575	266	1.00346	326	0.98769
27	0.98472	87	0.99811	147	1.01321	207	1.01565	267	1.00318	327	0.98750
28	0.98484	88	0.99840	148	1.01338	208	1.01555	268	1.00290	328	0.98731
29	0.98496	89	0.99868	149	1.01355	209	1.01544	269	1.00262	329	0.98712
30	0.98509	90	0.99897	150	1.01371	210	1.01533	270	1.00234	330	0.98694
31	0.98523	91	0.99926	151	1.01387	211	1.01522	271	1.00205	331	0.98676
32	0.98536	92	0.99954	152	1.01403	212	1.01510	272	1.00177	332	0.98658
33	0.98551	93	0.99983	153	1.01418	213	1.01497	273	1.00148	333	0.98641
34	0.98565	94	1.00012	154	1.01433	214	1.01485	274	1.00119	334	0.98624
35	0.98580	95	1.00041	155	1.01447	215	1.01471	275	1.00091	335	0.98608
36	0.98596	96	1.00069	156	1.01461	216	1.01458	276	1.00062	336	0.98592
37	0.98612	97	1.00098	157	1.01475	217	1.01444	277	1.00033	337	0.98577
38	0.98628	98	1.00127	158	1.01488	218	1.01429	278	1.00005	338	0.98562
39	0.98645	99	1.00155	159	1.01500	219	1.01414	279	0.99976	339	0.98547
40	0.98662	100	1.00184	160	1.01513	220	1.01399	280	0.99947	340	0.98533
41	0.98680	101	1.00212	161	1.01524	221	1.01383	281	0.99918	341	0.98519
42	0.98698	102	1.00240	162	1.01536	222	1.01367	282	0.99890	342	0.98506
43	0.98717	103	1.00269	163	1.01547	223	1.01351	283	0.99861	343	0.98493
44	0.98735	104	1.00297	164	1.01557	224	1.01334	284	0.99832	344	0.98481
45	0.98755	105	1.00325	165	1.01567	225	1.01317	285	0.99804	345	0.98469
46	0.98774	106	1.00353	166	1.01577	226	1.01299	286	0.99775	346	0.98457
47	0.98794	107	1.00381	167	1.01586	227	1.01281	287	0.99747	347	0.98446
48	0.98814	108	1.00409	168	1.01595	228	1.01263	288	0.99718	348	0.98436
49	0.98835	109	1.00437	169	1.01603	229	1.01244	289	0.99690	349	0.98426
50	0.98856	110	1.00464	170	1.01610	230	1.01225	290	0.99662	350	0.98416
51	0.98877	111	1.00492	171	1.01618	231	1.01205	291	0.99634	351	0.98407
52	0.98899	112	1.00519	172	1.01625	232	1.01186	292	0.99605	352	0.98399
53	0.98921	113	1.00546	173	1.01631	233	1.01165	293	0.99577	353	0.98391
54	0.98944	114	1.00573	174	1.01637	234	1.01145	294	0.99550	354	0.98383
55	0.98966	115	1.00600	175	1.01642	235	1.01124	295	0.99522	355	0.98376
56	0.98989	116	1.00626	176	1.01647	236	1.01103	296	0.99494	356	0.98370
57	0.99012	117	1.00653	177	1.01652	237	1.01081	297	0.99467	357	0.98363
58	0.99036	118	1.00679	178	1.01656	238	1.01060	298	0.99440	358	0.98358
59	0.99060	119	1.00705	179	1.01659	239	1.01037	299	0.99412	359	0.98353
60	0.99084	120	1.00731	180	1.01662	240	1.01015	300	0.99385	360	0.98348
										361	0.98344
										362	0.98340
										363	0.98337
										364	0.98335
										365	0.98333
										366	0.98331

Table 7
TM and ETM+ thermal band calibration constants

Constant	K1	K2
Units	W/(m^2 sr μm)	Kelvin
L4 TM	671.62	1284.30
L5 TM	607.76	1260.56
L7 ETM+	666.09	1282.71

Appendix

Table A1
To maintain consistency, all Landsat scenes are based on the following naming convention

Format Example: LXSPPPRRRYYYYDDDGSIVV L = Landsat X = Sensor S = Satellite PPP = Worldwide Reference System (WRS) Path RRR = WRS Row YYYY = Year DDD = Julian Day of Year GSI = Ground Station Identifier * VV = Version	**Sensor Examples:** LM10170391976031AAA01 (MSS) LT40170361982320XXX08 (TM) LE70160392004262EDC02 (ETM+)
*Ground Stations Identifiers - Data received at these sites are held at EROS	
AAA = North American site unknown ASA = Alice Springs, Australia FUI = Fucino, Italy (Historical) GLC = Gilmore Creek, AK, US HOA = Hobart, Australia KIS = Kiruna, Sweden MTI = Matera, Italy EDC = Receiving site unknown PAC = Prince Albert, Canada	GNC = Gatineau, Canada LGS = EROS, SD, USA, Landsat 5 data acquired by EROS beginning July 1, 2001 MOR = Moscow, Russia MLK = Malinda, Kenya IKR = Irkutsk, Russia CHM = Chetumal, Mexico XXO = Receiving site unknown XXX = Receiving site unknown

Table A2
Standard Level 1 product specifications

Product Type – Level 1T (Terrain Corrected) Pixel Size – 15/30/60 meters Output format – GeoTIFF Resampling Method – Cubic Convolution (CC) Map Projection – Universal Transverse Mercator (UTM) Polar Stereographic for Antarctica Image Orientation – Map (North Up) Distribution – File Transfer Protocol (FTP) Download only

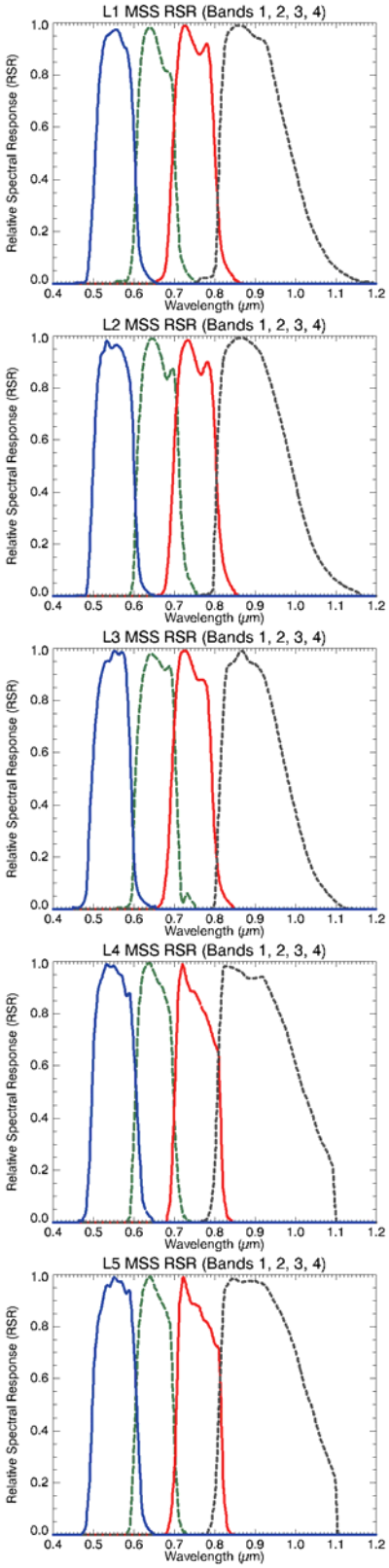

Fig. 1. Comparison of the solar reflective bands RSR profiles of L1–5 MSS sensors.

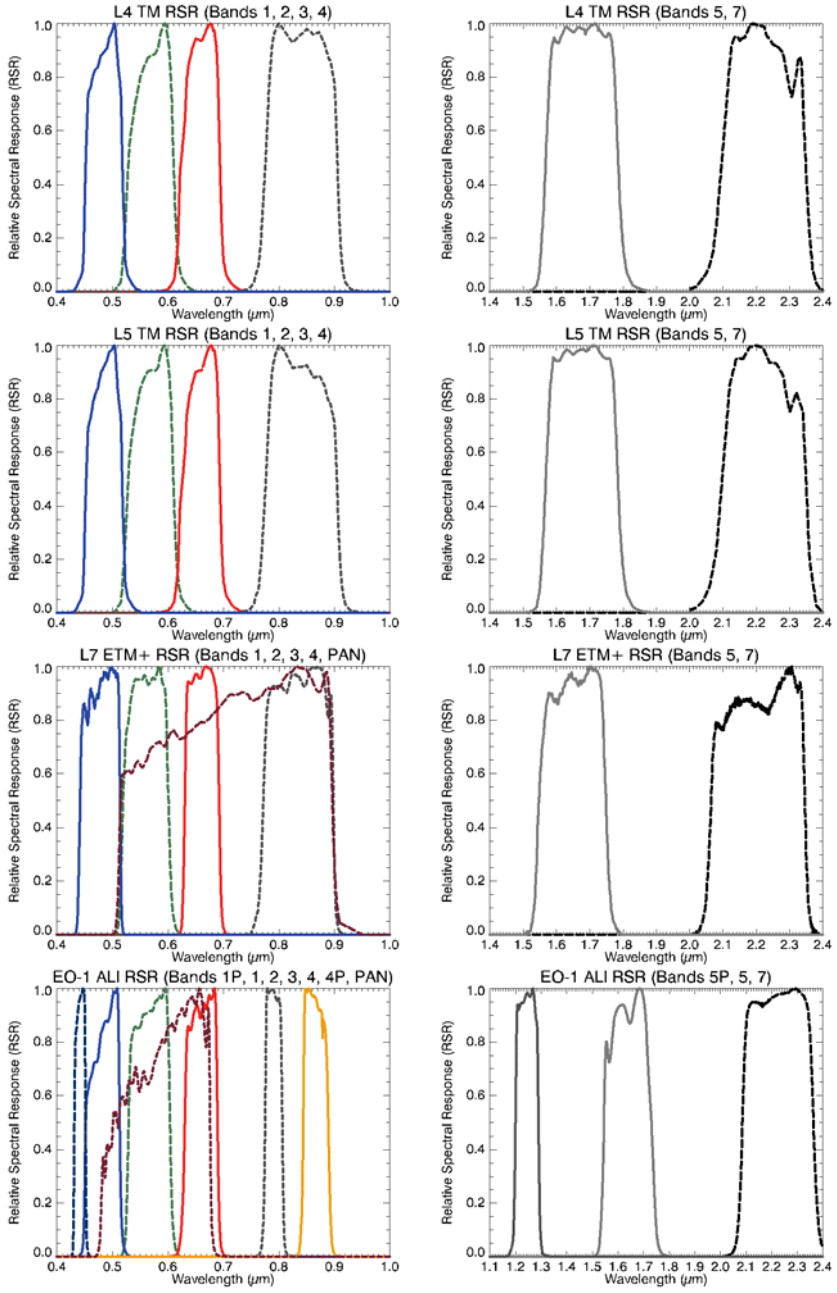

Fig. 2. Comparison of the solar reflective bands RSR profiles of L4 TM, L5 TM, L7 ETM+, and EO-1 ALI sensors.